The Journal of Experimental Biology 208, 3819-3834
Published by The Company of Biologists 2005
doi:10.1242/jeb.01765

The modulus of elasticity of fibrillin-containing elastic fibres in the mesoglea of the hydromedusa *Polyorchis penicillatus*

William M. Megill[1–3,*], John M. Gosline[1,2] and Robert W. Blake[1,2]

[1]*Department of Zoology, University of British Columbia, Vancouver, BC, V6T 1Z4, Canada,* [2]*Bamfield Marine Sciences Centre, Bamfield, BC, V0R 1B0, Canada* and [3]*Centre for Biomimetic and Natural Technologies, Mechanical Engineering Department, University of Bath, Bath, BA2 7AY, UK*

*Author for correspondence (e-mail: megillw@cerf.bc.ca)

Accepted 23 June 2005

Summary

Hydromedusan jellyfish swim by rhythmic pulsation of their mesogleal bells. A single swimming muscle contracts to create thrust by ejecting water from the subumbrellar cavity. At the end of the contraction, energy stored in the deformation of the mesogleal bell powers the refilling stage, during which water is sucked back into the subumbrellar cavity. The mesoglea is a mucopolysaccharide gel reinforced with radially oriented fibres made primarily of a protein homologous to mammalian fibrillin. Most of the energy required to power the refill stroke is thought to be stored by stretching these fibres. The elastic modulus of similar fibrillin-rich fibres has been measured in other systems and found to be in the range of 0.2 to 1.1 MPa. In this paper, we measured the diameters of the fibres, their density throughout the bell, and the mechanical behaviour of the mesoglea, both in isolated samples and in an intact bell preparation. Using this information, we calculated the stiffness of the fibres of the hydromedusa *Polyorchis penicillatus*, which we found to be approximately 0.9 MPa, similar in magnitude to other species. This value is two orders of magnitude more compliant than the stiffness of the component fibrillin microfibrils previously reported. We show that the structure of the radial fibres can be modelled as a parallel fibre-reinforced composite and reconcile the stiffness difference by reinterpreting the previously reported data. We separate the contributions to the bell elasticity of the fibres and mesogleal matrix and calculate the energy storage capacity of the fibres using the calculated value of their stiffness and measured densities and diameters. We conclude that there is enough energy potential in the fibres alone to account for the energy required to refill the subumbrellar cavity.

Key words: microfibril, modulus of elasticity, mechanical property, mesoglea, jellyfish, extracellular matrix, fibrillin, elastic fibre, *Polyorchis penicillatus.*

Introduction

Jellyfish swim by rhythmic pulsation of their mesogleal bell. Hydrozoan medusae, such as those of *Polyorchis penicillatus* Eschscholtz studied here, generally have a single circumferentially oriented swimming muscle that lines the underside of the bell, while scyphozoans generally have a second set of muscles oriented longitudinally, from shoulder to margin (Gladfelter, 1973). The swimming muscles contract to deform the bell and direct a quantity of fluid rearward through the velum. The animal is thereby propelled forward, either by jet propulsion in the case of prolate species such as *Polyorchis*, or, in more oblate species, through a drag-based mechanism reminiscent of sculling (Colin and Costello, 2002). Unlike squid, which have circumferential muscles to power the thrust stroke and radial muscles to power the refill (Gosline and DeMont, 1985), there is no muscle antagonist present in jellyfish medusae, so the refilling stage of the swimming cycle must be powered by passive energies stored in the deformation of the bell during the thrust phase (Gladfelter, 1972; DeMont and Gosline, 1988a; Megill, 2002). DeMont and Gosline (1988a–c) measured the material properties of the mesogleal tissue (a fibre-reinforced composite material), then the elastic behaviour of the whole bell, concluding that it was indeed possible to store enough energy in the bell to account for the refilling phase. However, they were not able to differentiate between the contributions of the mesogleal matrix and the mesogleal fibres. Since the mesogleal structure varies amongst jellyfish, it is important to identify which components of the structure are responsible for energy storage to fully understand the energetics of jet propulsive swimming in these organisms.

Polyorchis penicillatus (Fig. 1), also known as *P. montereyensis* (Rees and Larson, 1980), is a small (~1–5 cm long) hydrozoan jellyfish, found along the Pacific coast of North America from southern California to the Queen Charlotte Islands (Arai and Brinckmann-Voss, 1980) and southeast Alaska (Rees and Larson, 1980). The geometry of *Polyorchis* is shown in Fig. 1. The animal was described by Skogsberg

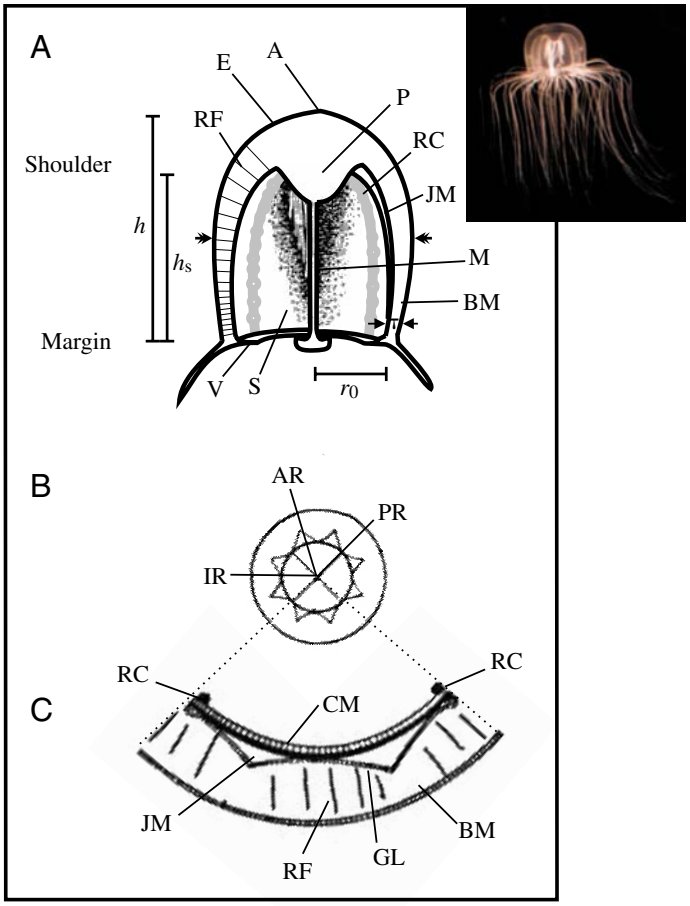

Fig. 1. *Polyorchis m*orphology. (A) Longitudinal section through the centre of the animal. (B) Cross-section taken at the location of the double-headed arrows in A. (C) Enlargement of one quadrant of B. The mesoglea is divided into two regions [labelled BM (bell mesoglea) and JM (joint mesoglea)] by the gastrodermal lamella (GL). During contraction, since the circumferential swimming muscle (CM) is only attached to the mesoglea at the per- [PR; at radial canals (RC)] and inter-radii (IR; away from RC), the bell first folds around the adradial joints (AR), and only later in the contraction begins to stretch the radial fibres (RF). Dimensions indicated are the bell height (h) from the apex (A) to the margin; shoulder height (h_s) between the shoulder and the margin; the radius at the base (r_0) and the wall thickness (τ). Other structures of interest: E, exumbrellar epithelium; S, subumbrellar epithelium; P, peduncle; M, manubrium; V, velum; RM, radial muscle. Drawings modified from Gladfelter (1972).

(1948) as generally cylindrical in shape, slightly longer from apex to margin than it is in diameter, with an average fineness ratio of 1.2. The conical, nearly hemispherical, apex of the bell consists of a large mass of mesoglea called the peduncle. The remainder of the animal is arranged cylindrically. In longitudinal section, the bell wall is tapered, radially thicker at the shoulder than at the margin. The swimming muscle is striated and consists of a layer of modified epithelial cells arranged circumferentially on the subumbrella. In *Polyorchis*, the muscle layer is only one cell thick (Gladfelter, 1972; Singla, 1978; Satterlie and Spencer, 1983; Spencer, 1995; Lin and Spencer, 2001), although in other species there can be extra folding of the muscle sheet to increase the cross-sectional area (Gladfelter, 1973). On the inside edge of the margin, there is a shelf (the velum) that extends radially inward to form a nozzle. A circumferentially arranged muscle on the subumbrellar side of the velum improves thrust generation by focussing the expelled jet of water and also allows the animal to steer (Gladfelter, 1972; Singla, 1978; Spencer, 1979). Tentacles extend radially off the outer edge of the margin, and a manubrium (digestive organ) extends from the base of the peduncle to the centre of the velar nozzle.

The passive mechanics of swimming, including energy storage and release, are determined by the properties of the mesoglea. Hydrozoan mesoglea is a hydrogel that contains mucopolysaccharides, collagen fibrils and other structural proteins, including microfibrils rich in a protein homologous to mammalian fibrillin (Bouillon and Vandermeerssche, 1957; Bouillon and Coppois, 1977; Gladfelter, 1972; Weber and Schmid, 1985; Reber-Müller et al., 1995). Fibrillar collagen type IV, fibronectin and heparansulfate proteoglycan have been reported from the mesoglea of *Hydra* sp. (Sarras et al., 1991), and laminin was identified in *Podocoryne carnea* (Beck et al., 1989) and *Hydra* sp. (Sarras et al., 1994). The collagen fibrils and fibrillin microfibrils are arranged in two intertwined fibrillar networks. Gladfelter (1972) describes the collagen network as '*a loose, three-dimensional lattice of cross-linked fibres enclosing pockets of both bound and free water*'. Weber and Schmid (1985) show a similar geometry for the microfibrillar network.

The bell of *Polyorchis penicillatus* is divided into two concentric layers of mesoglea separated by a sheet of cells called the gastrodermal lamella (Gladfelter, 1972). In the outer layer – the so-called 'bell mesoglea' – there is a radially arranged array of larger diameter fibres, which extend from the gastrodermal lamella to the exumbrellar epithelium (Chapman, 1959; Gladfelter, 1972; Weber and Schmid, 1985; DeMont, 1986; Reber-Müller et al., 1995, 1996). The fibres are multiply branched at each end and intertwine with the tissue layers to provide solid connections. Weber and Schmid (1985) showed these fibres to be microfibril bundles, and Reber-Müller et al. (1995) showed them to be rich in fibrillin. These fibres are reported to be 1.5–1.8 μm in diameter in fixed *Polyorchis* tissue samples (Gladfelter, 1972; Weber and Schmid, 1985), 0.03–1 μm in *Limnocnida* and 2–3 μm in *Pelagia* and *Aurelia* (Bouillon and Vandermeerssche, 1957).

The inner layer of mesoglea, called the 'joint mesoglea', is located between the gastrodermal lamella and the subumbrellar epithelium. It is less stiff and lacks the radially oriented elastic reinforcing fibres. There are thick fibres present (Gladfelter, 1972; Weber and Schmid, 1985), but these are sparsely distributed and arranged randomly. The joint mesoglea is divided into eight regions by the longitudinal interconnection of the subumbrella and gastrodermal lamella (Spencer, 1979). The regions are triangularly shaped in cross-section (Fig. 1), and their lower stiffness allows the bell mesoglea to fold around them during deflation (Gladfelter, 1972; Weber and

Schmid, 1985; DeMont, 1986). Most hydrozoans are similarly constructed (Gladfelter, 1973), although the thick-fibre array is less developed or absent in the bell mesoglea of species that do not actively swim (Gladfelter, 1973; Reber-Müller et al., 1996).

Modelling jellyfish mesoglea therefore as a fibre-reinforced soft tissue, we consider first the radially oriented fibres. Bouillon and Coppois (1977) showed that they could be made to stain for elastin, which led them to conclude that they are analogous in structure to vertebrate elaunin fibres, described by Kielty et al. (2002) as consisting of an outer microfibrillar sheath and an inner core of amorphous crosslinked elastin. However, since elastin seems to be limited to the vertebrates (Faury, 2001), Reber-Müller et al. (1995, 1996) speculated that there might well be an as yet unidentified elastic protein in the radial fibres. Similar speculation led Shadwick and Gosline (1985) to their discovery of octopus arterial elastomer (OAE), an analogous elastin-like protein in the circumferential fibres of octopus aorta.

There are, however, highly elastic fibres (oxytalan fibres) in vertebrates that lack the elastin core (Keene et al., 1991), such as mammalian zonular filaments (Sherratt et al., 2003) and the elastic fibres in foetal membranes (Malak and Bell, 1994). To stretch, these must rely either on the reorientation of *a priori* unaligned microfibrils (Lillie et al., 1994; McConnell et al., 1997) or on the inherent elasticity of the microfibrils themselves. Baldock et al. (2001) and Kielty et al. (2003) present a model of microfibril elasticity in which the fibrillin molecules unfold and refold, mediated by the level of Ca^{2+} (Wess et al., 1998; Eriksen et al., 2001).

It is possible that invertebrate elastic fibres are oxytalan-like in their construction – that is, they can be modelled simply as bundles of microfibrils. Indeed, Schmid et al. (1999) suggest that the elasticity in jellyfish radial fibres could be accounted for solely by the fibrillin microfibrils without the need for an elastin analogue. However, Sherratt et al. (2003) used a molecular combing technique to measure the stiffness of individual fibrillin microfibrils to be 78–96 MPa, nearly two orders of magnitude greater than the stiffness of the microfibril-rich fibres studied to date (~1 MPa). If their measurement is correct, and if the assumption can be made that invertebrate microfibrils are similar to those of vertebrate, then the low stiffness must be due to higher-order structure. The low relative stiffnesses of pig (Lillie et al., 1994) and lobster aorta (Davison et al., 1995), as well as sea cucumber dermis (Thurmond and Trotter, 1996), are all explained by the reorientation of the microfibril network present in the tissue. However, as pointed out by Wright et al. (1999), no similar explanation can be valid in the axially arranged microfibril bundles in the zonular filaments, nor in the jellyfish fibres discussed here. In jellyfish, the elastic fibres are oriented radially, parallel to (and, as we show in this paper, pre-tensioned in) the direction of applied stress. This geometry is similar to that in the vertebrate eye, and Wright et al. (1999) reported a non-linear (J-shaped) stress–strain behaviour for the zonular filaments in bovine eyes, with initial moduli between 0.07 and 0.27 MPa and final moduli between 0.47 and 1.88 MPa. Direct measurements of the mechanical properties of jellyfish fibres have not yet been made, but DeMont and Gosline (1988a) used Gladfelter's data on the density and cross-sectional area of *Polyorchis* fibres (Gladfelter, 1972) to predict, on the basis of energy storage arguments, that the modulus of the fibres should be approximately 1 MPa. This is well within the range of subsequent authors' measurements of the elastic modulus of similar fibres in other animals (Table 4). In this paper, we find the modulus of elasticity of jellyfish fibres to be approximately 0.9 MPa. The similarity of the results, coupled with the homology of their protein composition, suggests that invertebrate and vertebrate microfibrils are indeed similar.

The second component of the jellyfish bell is the gel, or mesogleal matrix. Several studies have been conducted on the chemical composition of the material (Chapman, 1966; Bouillon and Coppois, 1977; Weber and Schmid, 1985; Reber-Müller et al., 1995, 1996), but there are few measurements of its mechanical properties. Alexander (1962) studied the creep behaviour of mesoglea, but over long time frames (hours), by his own admission of little relevance to the animal's swimming behaviour (~1 Hz). DeMont and Gosline (1988a) studied the mechanical behaviour of mesoglea, both in isolated samples and in a novel intact animal preparation. They concluded that the overall tensile stiffness of mesoglea was between 400 and 1000 Pa but did not separate the contributions of the fibres and matrix. We present in this paper the first compression tests of jellyfish mesoglea and find the compressive stiffness, and hence stiffness of the extracellular matrix, of the joint mesoglea to be approximately 50 Pa. The bell mesoglea is stiffer in compression, approximately 0.35 kPa, and the tensile stiffness along the fibre axis is approximately 1.2 kPa.

Since there is no muscle to open the bell, the jellyfish mesoglea must be able to store enough energy during the thrust phase to power the refilling of the subumbrellar cavity. This energy must be stored in elastic deformation of the tissue. Gladfelter (1972) first proposed a mechanism by which this might happen, noting that the thickness of the mesogleal bell increased as the animal contracted its muscle, thereby stretching the radial fibres.

DeMont and Gosline (1988a) measured the energy required to refill the bell using experimental apparatus designed to mimic as closely as possible the deformation of the bell in free swimming. They sealed the subumbrellar cavity, then extracted water and measured the pressure generated. An integration of a polynomial curve fit to the resultant data gave them an estimate of the energy required to create the deformation. The mean energy requirement for 11 animals tested in this way was 4.6 μJ. They made corrections for dynamic loading at the animals' usual 1 Hz swimming frequency and for dissipative losses in the tissue, then calculated the required refill energy to be between 18 and 41 μJ.

To determine whether the radial elastic fibres could store the energy required, DeMont and Gosline (1988a) assumed the fibres to have a linear stiffness similar to that of elastin, then

used Gladfelter's measurement of the fibre density in *Polyorchis* (Gladfelter, 1972) to calculate the overall energy storage capacity of the fibres to be approximately 38 μJ, which is at the upper end of the calculated energy requirements. They concluded therefore that the fibres could store the energy and that their assumption of a stiffness similar to elastin was correct.

Gladfelter (1972) analysed the geometry of jellyfish bell during swimming. He showed that as the muscle contracts, it remains circular in cross-section, while the outer perimeter takes on a hexagonal cross-section due to the folding of the bell mesoglea around the wedge-shaped regions of joint mesoglea. The resulting elastic behaviour of the intact locomotor structure of the jellyfish is non-linear (DeMont and Gosline, 1988a; Megill, 2002), initially compliant as the bell mesoglea folds around the joints, then stiff once the fibres are stretched at the end of the contraction. The significance of this non-linear behaviour is that, during the early part of the contraction, more of the force generated by the muscle can go into expelling water, rather than into deforming the bell (Gladfelter, 1972). It also allows the muscle to power the refilling indirectly, by storing energy in the spring during a time in the contraction when it is still able to generate substantial tension but its ability to generate useful thrust is diminished due to a rapidly decreasing volume of water in the subumbrellar cavity (DeMont and Gosline, 1988b). The non-linearity complicates the analysis of the dynamics of the system, but DeMont and Gosline (1988c), using a linear approximation, were able to conclude that the animals were resonating, and Megill (2002) used a non-linear oscillator model to generalise that observation to jellyfish of all sizes.

In the current paper, we separate the contribution of the fibres from that of the matrix and conclude that the fibres have enough elastic energy storage capacity on their own to power the refilling of the subumbrellar cavity. We show that this enables the animal to increase the efficiency of its swimming mechanics by delaying the onset of energy storage to a later stage of the jet stage, when thrust efficiency drops off due to the decreasing volume of water in the subumbrellar cavity.

Materials and methods

Study animals

Live *P. penicillatus* (Fig. 1) were collected by SCUBA divers from the waters of Bamfield Inlet and Esquimalt Harbour, on the west coast of Vancouver Island, BC, Canada. Fibre diameter measurements were made at the Bamfield Marine Sciences Centre. Animals were kept there in running seawater aquaria until use. The remaining experiments were conducted at the University of British Columbia, so animals were shipped in chilled seawater and then held in a recirculating seawater aquarium until use. Aquaria in both locations were maintained at 11°C, and all animals were fed live *Artemia* every other day. Data from 68 of these animals, ranging in size from 16 to 42 mm (bell height), are presented in this paper.

Microscopy

Fibre density

To prepare samples for microscopy, the apex of the bell was first removed from the animal above the shoulder (Fig. 1). The resulting ring of muscle and mesoglea was then sliced longitudinally along one side to lay the animal out flat. Next, the flattened sample was laid on a pre-cooled microscope slide and quick-frozen using a spray refrigerant (1.1.1.2-tetrafluoroethane; MG Chemicals, Toronto, ON, Canada). Frozen samples were stored in a freezer until use. Samples were cut into 3–5 mm strips with a previously unused, frozen razor blade. The sections were then laid on a freezing microtome, sliced edges oriented down and up, such that the radial fibres were oriented parallel to the cutting surface, and shaven first on one side, then on the other, until the block of mesoglea was 500 μm thick. Finally, the microtome was turned off and allowed to warm up. As soon as the frozen sample had thawed sufficiently to release itself from the microtome stage, it was transferred carefully to a new microscope slide and covered with a cover slip.

Digital micrographs were taken of each sample using a video camera mounted on a Leitz (Wetzlar, Germany) Orthoplan interference contrast microscope, using 25× and 40× objectives and a first-order red filter to enhance the contrast. Images were captured on a microcomputer using a National Instruments (Austin, TX, USA) 1408 video capture board and LabView IMAQ software. Pixel dimensions were calibrated using micrographs taken at the same magnification of a stage micrometer (Bosch & Lomb, Rochester, NY, USA) with 10 μm line spacing.

Density was defined as the number of visible fibres intersecting a line across the micrograph, regardless of fibre diameter, divided by the width of the micrograph (40× objective, 640 pixels=128 μm; 25× objective, 640 pixels=206 μm), multiplied by the original thickness of the sample (500 μm). The fibre density calculation assumes that the shrinkage of the sample in preparation and handling was due only to the loss of water and matrix and that few fibres, if any, were lost. Although it was impossible to confirm this assumption, it seems reasonable given the high degree of intertwining and consequent solid anchorage of the fibres in the exumbrellar epithelium and gastrodermal lamella.

Fibre lengths

To measure the length of the fibres, a collage was made of adjoining 25× micrographs. Individual fibres were traced by hand using a computer graphics package (Corel Draw; Corel, Inc., Ottawa, ON, Canada). The tracings were converted to pixelated bitmaps and saved to disk. Custom-written software was then used to determine the length of the fibres by summing up the straight-line distances between the pixels. This calculation assumes that the fibres are lying in a plane and so must be interpreted as the minimum length. We applied a correction (described later) to take into account the irregular helical conformation reported by Gladfelter (1972) of the fibres in microscopy preparations.

Fibre diameters

Samples were prepared in a fashion similar to that used in the previous section but without the microtome. Approximately 3 mm-thick sections of mesoglea were sliced off the strip of mesoglea using a new razor blade. The sections were laid sliced side down on a microscope slide and covered with a cover slip. They were allowed to dry for 1 h before measurements were made, in order to facilitate focusing of the microscope. Measurements of diameter were made on the Leitz interference microscope with a 100× objective, oil immersion lens (N.A.=1.32), and a 15× filar ocular micrometer (Wild, Heerbrugg, Switzerland), at a total magnification of 1875×. The micrometer was calibrated with a stage micrometer (Bausch & Lomb, USA) with 10 μm line spacing.

Mechanical testing

Two mechanical tests were done to characterise the elastic behaviour of jellyfish mesoglea in radial tension. The first was done in air with a slab of isolated mesoglea, while the second was done underwater on an intact animal. Both experiments were done using an Instron (Canton, MA, USA) mechanical testing machine and a custom-built load cell. Morphological measurements (bell height, shoulder height, margin diameter and wall thickness – see Fig. 1) were made using callipers before testing.

Slabs of mesoglea were prepared and tested as follows. The apex was first removed by slicing the animal at the shoulder joint perpendicularly to its long axis. The resulting ring of muscle, skin and mesoglea was then sliced along one radial canal so that it could be laid flat on the moving stage of the testing machine (Fig. 2A). A 7×7 mm section of the stage (the lower grip) was covered with cyanoacrylate adhesive (Krazy Glue; Elmer's Products, Brampton, ON, Canada), and the mesogleal slab preparation laid over it such that one of the per-, ad- or inter-radii (Fig. 1) was centred on the grip. The dimensions of the grip and sample were selected to ensure that the edges of the sample were sufficiently distant from the grip to not interfere with the experiment. The stage was then raised until the upper surface of the mesogleal slab contacted a second, identically sized grip, itself connected to the load cell at the top of the testing machine frame. The stage was raised a little further, until 20 mN of force was applied to the mesogleal slab, to ensure that the glue set properly. The stage was lowered again after 10 s until the force returned to zero. This was set as the lower limit for the load cycles.

The self-loading of the tissue made it impossible to make a meaningful direct measurement of the resting thickness, τ_0. Furthermore, the action of pressing the sample against the grip to set the glue forced the joint mesoglea out of the wound at the shoulder and also caused some irreversible compression of the bell mesoglea. (20 mN of force corresponds to approximately 400 Pa of compressive stress on the sample, which was greater than the yield stress of the tissue.) The value of τ_0 was therefore back-calculated from the stiffness at high extension using a method identical to that of Lillie et al. (1994).

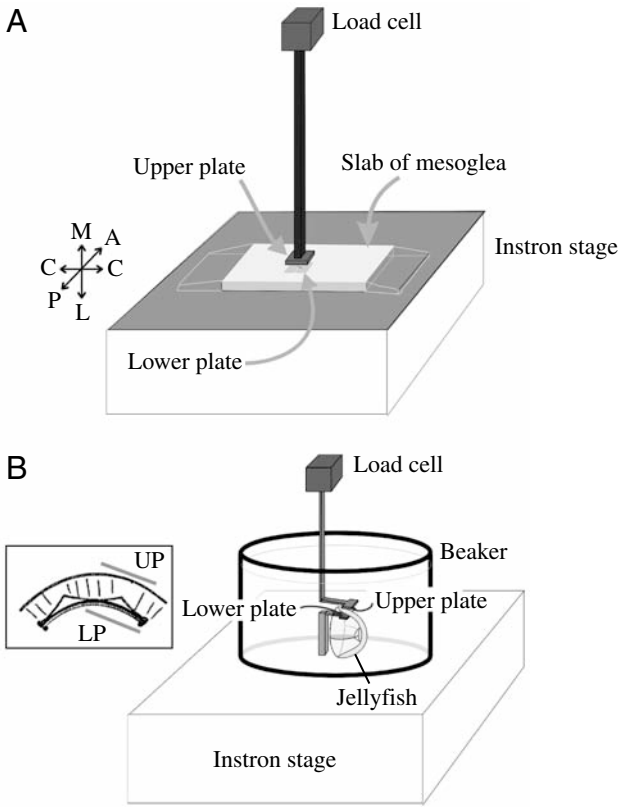

Fig. 2. Mechanical testing apparatus. (A) Isolated mesoglea preparation. A slab of mesoglea was laid on the moving stage of an Instron testing machine. Cyanoacrylate adhesive was applied to both plates. Orientation labels: A, anterior; P, posterior; M, medial; L, lateral; C, circumferential. (B) Intact animal preparation. Glue was applied to the bottom of the upper plate and the top of the lower plate. (Inset) Section looking along the long axis of the jellyfish in the mount. Plates were aligned over the ad-radius (as shown) or per-radius.

A linear regression was fit to the loading curve at high extension, and the point at which the regression line crossed the x-axis (zero stress) was taken to be τ_0. Once τ_0 had been determined, the extension data were converted to engineering strain ($\epsilon=\Delta\tau/\tau_0$). Engineering stress and strain are approximations to true stress [force (F) / instantaneous area (A)] and strain [extension (dx) / instantaneous extension (x)]. They are related to their true counterparts by:

$$\epsilon_{\text{eng}} = \int_{\tau_0}^{\tau} \frac{1}{x}\,\mathrm{d}x = \ln(\tau_0)\epsilon_{\text{true}}\,,$$

$$\sigma_{\text{eng}} = F\frac{A_0}{A}\,. \qquad (1)$$

Engineering stress and strain are precise only for small extensions. The consequence of using engineering quantities is that the stiffness in compression will be overestimated, while that in tension will be underestimated. However, the error introduced by using these small deformation approximations (~5%) is less than the experimental uncertainty (~15–20%)

introduced due to the highly compliant, easily deformable nature of the materials under test.

In order to measure the stiffness of the joint mesoglea, a second, intact animal preparation was designed (Fig. 2B). A 7 mm square plate of polystyrene was glued to an L-shaped rod suspended from the load cell. A second identical polystyrene plate was cantilevered from a post fastened through the base of a plastic beaker to the Instron stage. The beaker was filled with 11°C seawater to a level just below the lower plate. Cyanoacrylate adhesive (Krazy Glue) was applied to the plate, and the jellyfish positioned over the plate, as shown in Fig. 2B, such that one of the per-, ad- or inter-radii was centred on the plate. The glue was given 20 s to set before additional seawater was added to raise the level to just below the outer (now upper) edge of the mesogleal bell. Cyanoacrylate adhesive was applied to the bottom of the upper plate. The stage below the beaker was then raised until the upper plate came in contact with the exumbrellar surface of the jellyfish. The stage was raised a little further, until 20 mN of force was applied to the jellyfish, to ensure that the glue set properly. After 10 s, seawater was added until the jellyfish was completely submerged. The stage was then lowered until the force returned to zero. As before, this was set as the lower limit for the load cycling. The resting thickness, τ_0, was calculated as above for the isolated slabs.

In both cases, the sample was loaded in tension at 10 mm min^{-1} to various strains between 5 and 40% [to span the range of radial strains measured by Gladfelter (1972) in live swimming animals], although if the latter was not enough to cause the sample to yield, experiments were continued at increasing strains until it did yield. Stress was defined as the load divided by the surface area of the polystyrene plates (engineering stress), and strain was defined as the extension divided by the resting thickness, τ_0 (engineering strain).

Statistical tests were carried out following Zar (1984) and Dixon and Massey (1983). Unless otherwise noted, results are given as means ± S.E.M. (standard error of the mean).

Results

Jellyfish morphology

Measurements were made, as defined in Fig. 1, of the bell height (h) and margin radius (r_0) of 67 animals. Data for an additional 12 animals were extracted from Gladfelter (1972). Measurements were also made of the wall thickness (τ) and shoulder height (h_s) of 43 jellyfish. Data were not normally distributed, so a non-parametric test (rank correlation; Dixon and Massey, 1983) was used to test correlation. There was a weak negative correlation of fineness ratio (r_0/h; r_s=–0.30, N=79, P<0.05) and shoulder ratio (h_s/h; r_s=–0.29, N=43, P<0.05) and no correlation of wall thickness ratio (τ/h; r_s=0.05, N=43, P>0.05) to bell height for the animal size range studied in this paper (Fig. 3). We assume, therefore, that for the size range studied in this paper (7 mm<h<40 mm), wall thickness can be assumed to scale geometrically. Mean wall thickness was 0.13h (±0.03h, N=43). The fineness and shoulder height

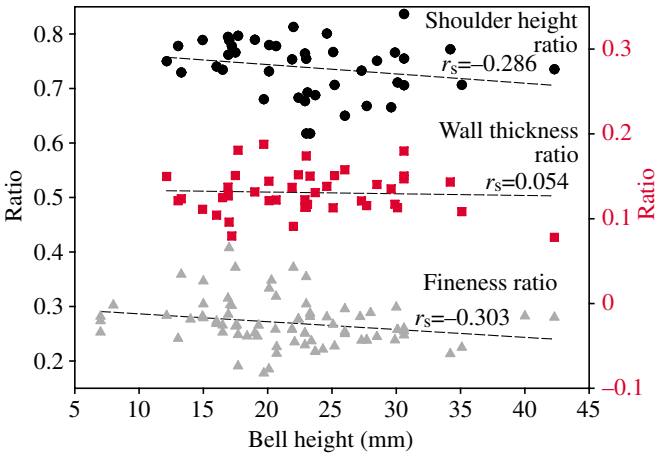

Fig. 3. Scaling of bell geometry with bell height. Shoulder height (h_s/h) and fineness (r_0/h) ratios are plotted on the left-hand vertical axis, while the wall thickness ratio (τ/h) is plotted on the right-hand axis. Shoulder height and fineness ratios decrease with increasing bell height. The slopes of both lines were significantly different from zero (P<0.05 for both). The wall thickness ratio did not scale with bell height.

ratios for the animals studied in this paper were decreasing functions of bell height – that is, larger animals tended to be more elongate and their peduncles tended to be longer.

Fibre morphology

Fibres were oriented more or less perpendicularly to the ex- and sub-umbrellar surfaces and traversed most of the thickness of the bell, anchored in the exumbrella by intertwining with the fibres there, as observed by other workers (Gladfelter, 1972; Weber and Schmid, 1985; Reber-Müller et al., 1995). Near the gastrodermal lamella, they branched multiply into finer and finer fibres, presumably anchoring themselves in the lamella, though this could not be discerned using the available microscope. Branching began about halfway across the thickness of the bell. Because of the preparation procedure (freezing and thawing), the sample tended to leak and shrink substantially, with a loss of radial thickness typically of ~40%. When viewed through the microscope, the fibres were slack (Fig. 4). Because the fibres assume an irregular helical conformation when slack (Gladfelter, 1972), it was not possible to measure their exact length from the micrograph. However, a minimum estimate can be obtained by assuming the fibres to lie in a plane. The mean length of the crimped planar projection of the six fibres highlighted in Fig. 4 was 0.64±0.01 mm (N=6). To correct for the non-planar conformation of the fibres, we assume that they are as crimped in depth as they are in planar projection. The radial thickness of the exumbrellar mesoglea in Fig. 4 was approximately 0.5 mm. The ratio of the folded to unfolded length of the fibres was therefore 0.64 mm/0.5 mm=1.28. This gives a corrected mean fibre length of 0.82 mm. The total radial thickness of the collage shown in Fig. 4 is 1.35 mm. The animal's measured resting wall thickness was 3.0 mm, indicating a 55% loss of

radial thickness due to water loss. Thus, if the water loss was uniform throughout the animal, the corrected thickness of the outer mesoglea was approximately 1.11 mm, suggesting an *in vivo* pre-strain of the fibres of ~35%. This is obviously an educated guess, but it does partially confirm the speculation by previous authors that the fibres were probably pre-strained *in vivo* (Bouillon and Vandermeerssche, 1957; Chapman, 1959; Gladfelter, 1972; DeMont, 1986).

Fibre diameters

Fig. 5D is a typical micrograph of the mesogleal fibres. 1400 measurements were made of 350 fibres in 10 jellyfish – data are presented in Fig. 6 and summarised in Table 1. Sections of mesoglea were taken from inter-, per- and ad-radii, and no significant differences (ANCOVA, F=0.012, $F_{0.975,2,14}$=4.46, P>0.05) were found between regions or animals – that is, the change in fibre diameter scaled identically with bell height in all three regions for all animals. All measurements were therefore pooled into one regression, given by d_f=1.35+0.05h (μm). Using the pooled regression, the predicted unbranched fibre diameter for a 'standard' animal of h=20 mm [corresponding to the size of the jellyfish used by DeMont and Gosline (1988a) to calculate the energy required to refill the bell] was 2.34±0.41 μm (95% confidence intervals at h=20 mm). This is substantially larger than the 1.5 μm reported by Gladfelter (1972) and the 1.8 μm reported by Weber and Schmid (1985). Neither reported how the measurements were made, nor from animals of what size, nor did they give a range. However, Gladfelter's and Weber and Schmid's measurements were made on histological preparations, so it is most likely that the dehydration of the fibres accounts for their smaller dimensions.

Fibre densities

Fig. 5A–C shows a typical set of micrographs used to measure fibre densities. Samples were taken from eight jellyfish ranging in size from 17.7 to 42.3 mm bell height. Fibre densities were highest at the ad-radius, followed by the per- and then the inter-radii. Consistent with Gladfelter (1972), the density of fibres was greatest near the gastrodermal lamella (subumbrellar side) and least near the exumbrellar side (Fig. 4). The higher density near the gastrodermal lamella was due to the high degree of branching in that region. Only micrographs from the mid-thickness region of the bell wall, where fibres were mostly unbranched, were used in the calculation of the mean fibre

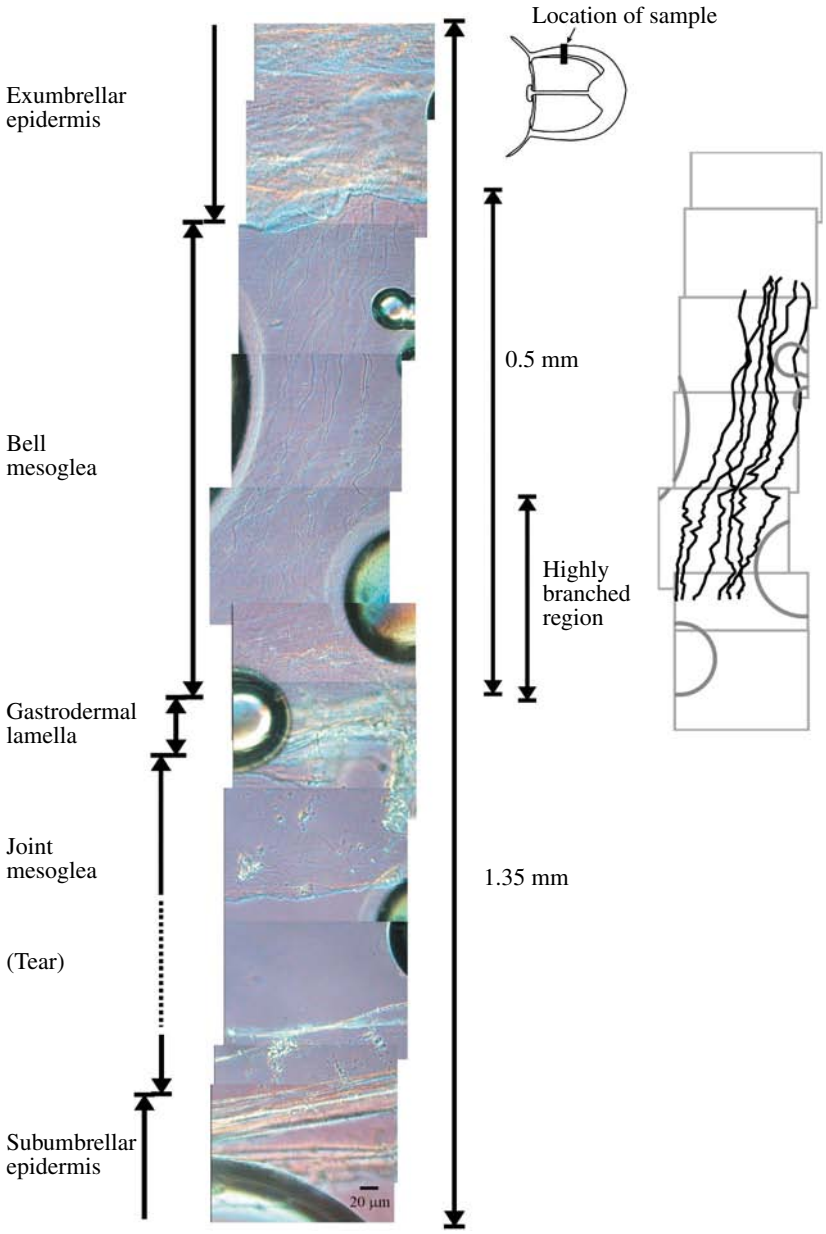

Fig. 4. Collage of micrographs showing a complete cross section of a jellyfish. Micrographs were taken using a video capture system and a 25× objective on an interference contrast microscope. Fibres can be traced from the inner edge of the exumbrellar epidermis to the gastrodermal lamella. Note the high degree of branching of the fibres at their ends, and the intertwining of the fibres with the tissue of the exumbrellar epithelium and the gastrodermal lamella. Also note the coiled, slack appearance of the fibres in the medial half of the bell mesoglea and the absence of organisation in the fibres of the joint mesoglea. The black rimmed circular structures in the micrographs are air bubbles introduced during the thawing and transfer of the sample from the microtome to a microscope slide. (Inset) Tracings of the six fibres from gastrodermal lamella to exumbrella. Air bubbles are shown for orientation. The path lengths of the tracings were calculated, and a correction (described in text) applied to derive a reasonable minimum estimate of the unstressed length of the fibres. Note that the tracings follow a single branch of the fibre in the highly branched region near the gastrodermal lamella.

densities. The distribution of fibre density over the cylindrical section of the bell is reported in Table 2. In all regions, the fibre density decreased with bell height (Fig. 7). No significant differences were found between regions in the regression slopes of density against bell height (ANCOVA, $P>0.05$), so the data were pooled, and an overall regression slope fitted to the data. For the range of jellyfish studied, density (n) was found to scale linearly with bell height following the equation $n=322–5.5h$ (mm^{-2}). For the 'standard' jellyfish of 20 mm bell height, the fibre density is predicted to be 212±34 mm^{-2}.

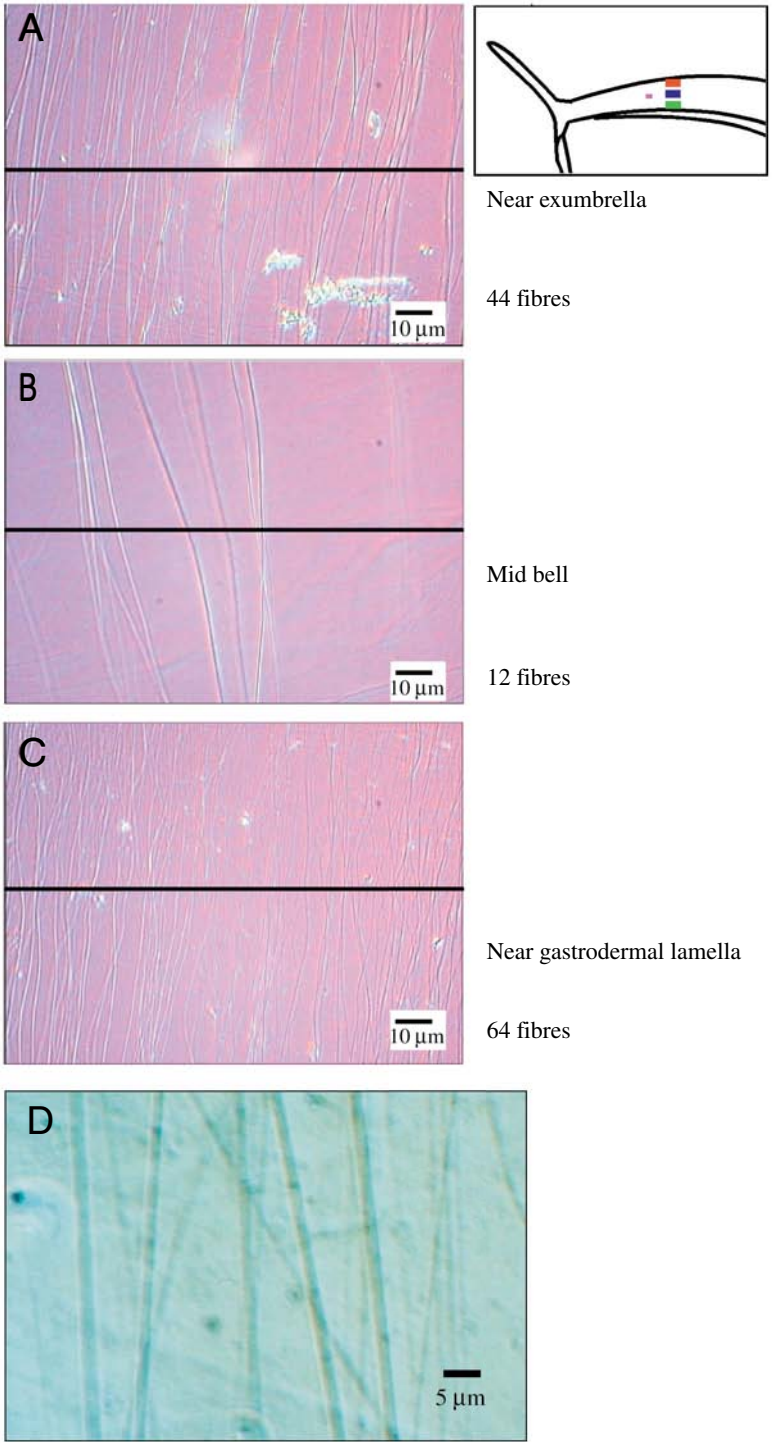

Fig. 5. (A–C) Micrographs used to measure the density of jellyfish microfibrils. Micrographs taken with a video capture system using a 40× objective on an interference contrast microscope. Samples were allowed to dry down for an hour before measurements were taken, to facilitate focussing the microscope. Fibres were branched at both ends, more so at the medial end, near the gastrodermal lamella. (A) Near the exumbrellar surface. (B) Mid bell. (C) Near the gastrodermal lamella. Fibre density was determined by counting the number of fibres crossing the black line across the micrograph. Micrograph width: 640 pixels=128 μm. Depth of sample: 500 μm. (D) Digital micrographs taken with a 100× objective on the interference contrast microscope show that fibre diameter increases slightly with body size. For improved accuracy, measurements were made with a 15× filar micrometer eyepiece mounted on the microscope. (Inset) Approximate locations and orientation of samples are indicated by the coloured boxes: red, A; blue, B; green, C; magenta, D.

Mechanical properties of mesoglea

A total of nine individual jellyfish were tested using one or both of the protocols described earlier. Six animals were tested using the isolated slab procedure only, two were tested using both methods, and one was tested using the whole animal method only. We report data for the 11 tests in Table 3.

Fig. 8A shows a typical result of a radial test of an isolated slab of mesoglea. Negative strains indicate that the sample is being tested in compression, while positive strains indicate tension. Because the joint mesoglea was forced out of the sample during the glue-setting step at the beginning of the experiment, the compressive stiffness measured was that of the dense fibre-reinforced bell mesoglea. In the plane transverse to the fibres, the tissue is isotropic, so the compressive stiffness of the mesoglea is also the tensile stiffness of the bell mesogleal matrix. The mean modulus of elasticity of the bell mesoglea, E_m, was 344±52 Pa. The stiffness of the material was higher in tension, reflecting the fibre-reinforcement of the mesoglea in the radial direction. Data for the six jellyfish tested in this manner are presented in Table 3 (animals 19–24). The mean stiffness of the mesoglea in radial tension, E_L, was 974±162 Pa.

Typical results of the intact animal tests are shown in Fig. 8B. Data for the three animals tested in this manner are shown in Table 3 (individuals 25–27). The tensile stiffness, E_L, of the intact preparation was similar to that of the isolated preparations, but because the joint mesoglea is much less dense than the bell mesoglea (Gladfelter, 1972) and remained intact during the test, the compression stiffness was much lower than in the isolated preparation. The mean compressive stiffness of the mesoglea, E_c, was 130±11 Pa. We make use of this value in the Discussion to derive an estimate of the stiffness of the joint mesoglea.

Table 1. *Fibre diameters*

Individual	Bell height (mm)	Fibre diameter ($\times10^{-6}$ m) Mean ± S.D.	*N*
9	24.6	2.16±0.50	40
10	30.6	3.22±1.12	30
11	19.0	2.56±0.81	30
12	28.5	2.80±0.50	30
13	29.9	2.63±0.70	30
14	34.2	3.07±0.57	30
16	23.8	3.36±1.36	51
17	26.7	2.63±0.65	20
Predicted	20.0	2.34±0.41	

Data are the means ± S.D. of fibre diameters measured using a 100× objective and a 15× filar micrometer on an interference contrast microscope. Analysis of the covariance shows the fibre diameter to be an increasing function of bell height, but not of bell region (F=0.012, $F_{0.975,2,14}$=4.46, P>0.05). Data were therefore pooled into a single regression (Fig. 6) given by d_f=1.35+0.05h (μm). The predicted value is given for the 'standard' jellyfish of bell height 20 mm. The range reported for the prediction is the 95% confidence interval of the regression at that bell height.

Two animals (25, 27) were tested both ways. After the intact animal test, slabs of mesoglea were cut from the animals and tested in isolation. Neither the compressive stiffness, E_m, nor the radial tensile stiffness, E_L, were different from those of previously tested animals, so all data were combined to give overall averages of E_m=352±39 Pa and E_L=1186±159 Pa.

Table 2. *Fibre densities*

Individual	Bell height (mm)	Fibre densities (mm^{-2}) IR	PR	AR
1	35.1	151	92	122
2	22.9	229	341	162
3	30.6	100	145	127
4	20.1	126	178	200
5	42.3	85	123	103
6	17.7		317	206
7	27.3	183	148	100
8	30.6	193	167	160
Predicted	20.0		212±34	

Data are the mean fibre densities in the unbranched regions of the ad-, per- and inter-radii. Fibre densities were calculated by counting the number of fibres, regardless of diameter, intersected by a horizontal line across a 25× micrograph (see Fig. 4), divided by the original area of the sample (206 μm×500 μm). IR, inter-radius; PR, per-radius; AR, ad-radius. There is a weak negative correlation of fibre density on bell height. Predicted density is for the 'standard' jellyfish of 20 mm bell height, corresponding to the animal size used by DeMont and Gosline (1988a) to calculate the energy required to refill the bell. Note that the densities presented in this table were calculated in a manner different from the one used by Gladfelter (1972), so the data cannot immediately be compared.

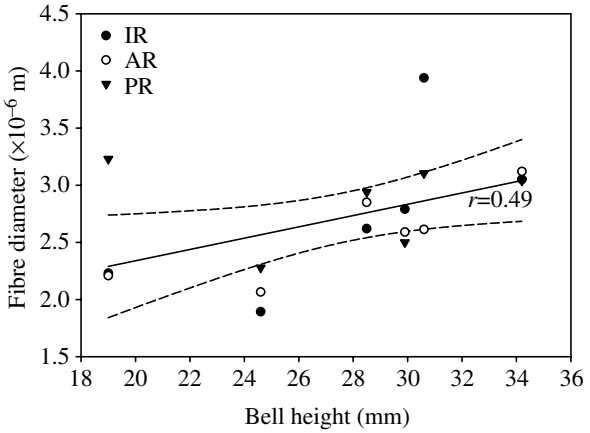

Fig. 6. Fibre diameter as a function of bell height. Data are plotted for the inter- (IR), ad- (AR) and per- (PR) radius regions. Regressions for all regions of diameter against bell height were significantly different from zero, but there was no difference between the slopes for the three regions. Data are therefore pooled and a single regression is plotted, along with its 95% confidence intervals (broken lines). The slope of the line is d_f=1.35+0.05h (μm). For the 'standard' jellyfish of 20 mm bell height, the predicted fibre diameter is 2.86±1.03 μm.

Discussion

We have made detailed measurements of the distribution and morphology of the radial elastic fibres in the mesoglea of the hydromedusa *Polyorchis penicillatus*. We have shown that the fibres are probably pre-strained *in vivo*, consistent with other authors' observations (Gladfelter, 1972; Weber and Schmid, 1985). We have found that the fibre diameter increases very slightly with bell size, while the density of the fibres decreases as the animal grows. We have set our morphological observations in a mechanical context by measuring the stiffness

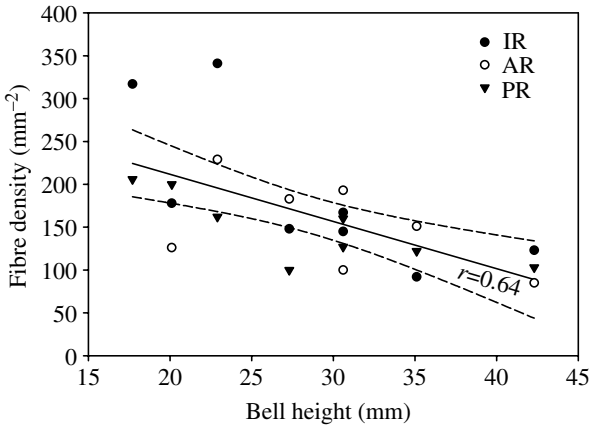

Fig. 7. Fibre density as a function of bell height. The density of radial fibres decreased with body size in all areas of the bell. There was no significant difference in the slopes between regions, so data were pooled and a single regression plotted, together with its 95% confidence intervals (broken lines). The slope of the line is n=322–5.5h (mm^{-2}). The fibre density of the 'standard' jellyfish (bell height = 20 mm) is predicted to be 212±34 mm^{-2}.

Table 3. *Elastic moduli of jellyfish mesoglea in radial tension*

Individual (region)	Bell height (mm)	Wall thickness (mm)	τ_0 (mm)	E_m (Pa)	E_{jm} (Pa)	E_L (Pa)	
						Isolated	Intact
19	20.7	3.1	2.19	258		826	
20	19.2	2.7	1.83	451		1493	
21	19.3	2.3	2.09	488		978	
22	17.1	2.6	1.99	441		1338	
23	17.7	3	1.70	214		400	
24	18.4	2.6	2.32	216		806	
25	22.1	3.5	4.39	350	111	1241	1094
26	16.5	2.4	2.89		149		1699
27	17.6	2.9	4.08	400	131	1897	1730
Mean				352	130	1186	
S.E.M.				39	11	159	

E_{jm} is the compression stiffness of the joint mesoglea during intact animal tests. E_L is the stiffness of the system in tension and represents the contributions of both the matrix and fibres. Data for individuals 19–24 were obtained from isolated tissue tests, and those for individual 26 were obtained from intact animal tests. Mesoglea from individuals 25 and 27 was tested both ways. There was no discernible difference in E_L between the two methods. To obtain τ_0, we fit a straight line through the highest reasonable loading slope on a graph of stress as a function of extension, and tracked it to zero stress. The abscissa was taken as τ_0. This usually lay somewhere near the inflection point in the loading curve. Due to the practical limitations of the testing apparatus, only jellyfish of approximately 2 cm bell height could be tested. Hence, no trend with size can be reported. We have therefore grouped all of the data together into a single mean and have limited our conclusions to jellyfish of this size range.

of both types of mesoglea, both in tension and in compression – our result for the compressive stiffness of the bell mesoglea is similar to that found by DeMont and Gosline (1988a). In this section, we discuss the implications of our morphological observations, then calculate the stiffness of the fibrillin-rich elastic fibres in the mesoglea of *P. penicillatus*. Next, we present several models of the mechanical behaviour of the radial fibres, which we use to generate hypotheses to explain how bundles of apparently stiff microfibrils can be two orders of magnitude less stiff than their component parts. Finally, we show that there is enough energy storage potential in the fibres to power the refill stage of the jet cycle, and that this potential is available in the latter stages of the contraction. We suggest that this design exists to minimise the energy that the muscle has to provide for refill during the active thrust production stage of the jet cycle by shifting the energy storage stage to a time in the jet cycle when the muscle can no longer produce useful thrust due to the rapidly diminishing subumbrellar volume.

Scaling

We have shown that the wall thickness of *Polyorchis* scales linearly with bell height (i.e. the ratio of wall thickness to bell height is constant over the range of sizes studied; Fig. 3). The polyp of *Polyorchis*, if it exists, remains undiscovered (Brinckmann-Voss, 2000) but, by comparison with other species, it can be assumed that young medusae are of the order of 1–2 mm in bell height when they first appear. We found medusae whose bell height exceeded 45 mm. If the geometric scaling assumption is true, then the outer mesogleal thickness increases from a few dozen microns to more than 5 mm. We did not make measurements of the fibres in very small medusae, but it seems reasonable to assume that the fibres extend from the gastrodermal lamella to the exumbrella as they do in larger individuals, particularly as this is the case in other hydromedusae (Reber-Müller et al., 1995). The implication of all of this is that the fibres increase in length by 10–100-fold as the animal grows, which implies that they must grow, rather than simply stretch, which in turn implies that additional fibrillin microfibrils must be added to the radial fibres as the medusa grows. The decrease in fibre density with size (Fig. 7) suggests that new fibres are not added, but rather that the existing fibres grow. The additional microfibrils might come from the three-dimensional fine microfibrillar network in the surrounding mesoglea, rather than be laid down *de novo*.

The alternative explanation is that the fibrillin scaffolding is laid down first, and not added to. The extra fibre length would then be postulated to come from the addition of some jellyfish mesogleal elastomer. The prediction in this case would be that the stiffness of the fibres should decrease with size. Owing to practical constraints imposed by our testing apparatus, we did not make any measurements of the stiffness of small or large animals, but it would be interesting to do so.

Stiffness of the joint mesoglea

Due to the watery composition of jellyfish joint mesoglea, we were not able to make a direct measurement of its stiffness. However, we were able to derive an estimate of the stiffness of this highly compliant material by proceeding as follows. We measured the compressive stiffness of intact combined joint and bell mesoglea and found it to be 131±11 Pa. The thickness of the joint mesoglea is not constant around the circumference of the bell, but rather wedge-shaped, thinner near the radial

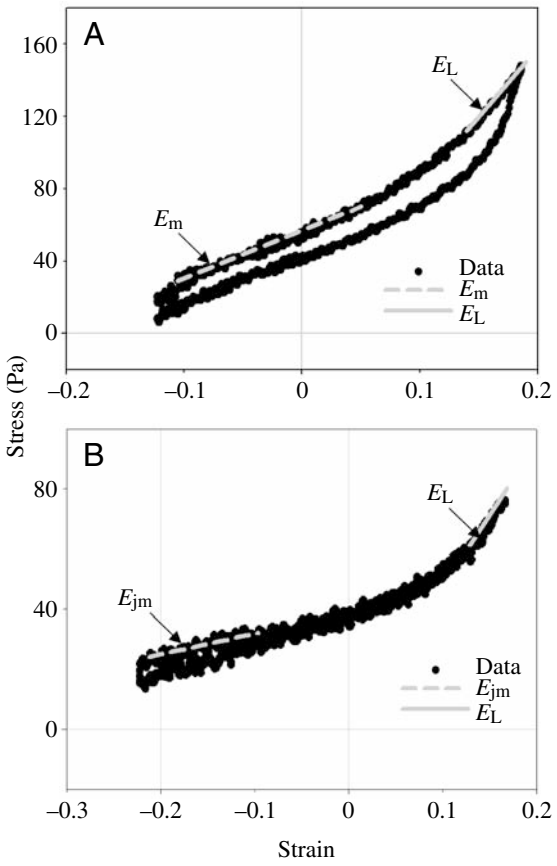

Fig. 8. (A) Typical stress–strain behaviour of a slab of isolated mesoglea in the radial direction. The figure is constructed from the first load and unload cycle to avoid errors due to tissue damage and degradation during the experiment. Negative strains represent compressive loading, while positive strains indicate tension beyond the resting thickness. The sample was compressed below its resting thickness during mounting, with the result that the fibres, normally pre-strained *in vivo*, were slack. The joint mesoglea was removed in this preparation, so it was possible to measure the stiffness, E_m (broken line), of the bell mesoglea alone. The stiffness is the slope of a straight line fit to the data in the region between the extension and compression shoulders. The solid line shows the parallel stiffness, E_L, which includes contributions from matrix and fibres. Again, the stiffness was determined from the slope of a line fit to the straight line region near the ultimate strain, defined as the strain just before the tissue began to yield. For most jellyfish, the ultimate strain was approximately 35%, which corresponds well to the 36% radial strain observed by Gladfelter (1972) during swimming. Data for eight jellyfish tested in this manner are summarised in Table 3 (the data shown in this figure are from Jellyfish 19). Zero strain was determined by regressing from the large strain data, as discussed in the Materials and methods. Following Lillie et al. (1998), stiffnesses were determined using the loading curve rather than the unloading curve. The hysteresis in the isolated preparation is probably due in large part to water loss during the experiment. (B) Typical stress–strain behaviour of intact mesoglea. Negative strains represent compressive loading, while positive strains indicate tension beyond the native thickness. Because there was no loss of joint mesogleal tissue in this preparation, the slope of the broken line is the upper limit (as discussed in the text) of the stiffness of the joint mesoglea, E_{jm}, while the slope of the solid line is again the radial tensile stiffness parallel to the fibres and includes contributions from the matrix and fibres. Data for three jellyfish tested in this manner are summarised in Table 3 (data in this figure are from Jellyfish 25). As in A, zero strain was determined from a regression through the large strain data.

canal (per-radius) and inter-radius than in the adradial region (Fig. 1). The triangular shape of the joint mesogleal wedge has the effect of increasing the effective stiffness measured during the experiment (since the resting thickness, τ_0, is not constant). The value we measured was therefore an upper limit. An exact correction factor would depend on the shape of the wedge, which we did not measure, but, based on Gladfelter's drawing (Gladfelter, 1972) and the relative sizes of the jellyfish and testing plate (Fig. 2, inset), we can estimate that the stiffness of the joint mesoglea, E_{jm}, is about one-third of the combined stiffness, or approximately 50 Pa. This is a factor of seven less than the stiffness of the bell mesoglea (E_m=352 Pa), which helps to explain how the buckling is controlled during the thrust phase of locomotion.

Radial fibre stiffness

The stiffness of the radial fibres can be calculated from the tensile stiffness of the bell mesoglea by accounting separately for contributions by the fibres and matrix to the overall elasticity (McConnell et al., 1997). Because the radial fibres traverse the entire bell wall (Fig. 4), the mesoglea can be modelled as a continuous parallel composite (*sensu* Lillie et al., 1998):

$$\sigma = [E_f V_f + E_m(1 - V_f)]\epsilon \,, \quad (2)$$

where E_f and E_m are the moduli of the fibres and matrix, respectively, and V_f is the unitless volume fraction of fibres in the mesoglea, given by:

$$V_f = \tfrac{1}{4}\pi d_f^2 n \,, \quad (3)$$

where d_f is the fibre diameter, and n is the fibre density. Assuming a 'standard' fibre density of 212 mm^{-2} and a 'standard' fibre diameter of 2.34 μm, the fibre volume fraction was approximately 0.091%. Rearranging Eqn 2 and substituting in the combined stiffness, E_L=σ/ϵ, of the mesoglea, gives:

$$E_f = [E_L - E_m(1 - V_f)]/V_f \,. \quad (4)$$

Assuming a mean E_L of 1186 Pa and a mean E_m of 352 Pa, the fibre modulus for the 'standard' jellyfish is approximately 0.92 MPa (range 0.44–1.98 MPa, derived using the mean ± 1 S.E.M. for the stiffnesses and the 95% CIs for the fibre diameter and fibre density). For comparison, reported stiffnesses for analogous fibres in other animals range from 0.2 to 1.9 MPa (Table 4). Our measurement of the stiffness of jellyfish radial fibres falls in the middle of that range.

Towards a model of fibre elasticity

Elastic fibres such as those in jellyfish mesoglea play an important role in the mechanical behaviour of biological soft

Table 4. *Moduli reported in the literature for analogous elastic fibres*

Organism	Tissue	Modulus	Reference
Cow	Zonular filaments	0.19–1.88 MPa	Wright et al. (1999)
Jellyfish	Mesogleal fibres	0.9 MPa	Present study
Lobster	Aorta fibres	1.06 MPa	McConnell et al. (1996)
Octopus	Aorta fibres	0.4 MPa	Shadwick and Gosline (1985)
Pig	Aorta fibres	0.4 MPa	Lillie et al. (1998)
Sea cucumber	Dermis network	0.2 MPa	Thurmond and Trotter (1996)
	Elastin	1.2 MPa	Aaron and Gosline (1981)
	Microfibrils	78–96 MPa	Sherratt et al. (2003)

tissues. The factor of seven greater stiffness of (fibre-reinforced) bell mesoglea over (fibre-free) joint mesoglea highlights this role, as do the serious cardiovascular, ocular and skeletal consequences of genetic disruption of the structure of elastic fibres in humans (Marfan's syndrome; for reviews, see Robinson and Godfrey, 2000; Milewicz et al., 2000). It is important therefore to understand the origin of elasticity of the fibres. To do this, we must understand the fibre structure and material properties of its constituent components.

A jellyfish radial fibre is itself a fibre-reinforced composite. Scanning electron micrographs presented by Weber and Schmid (1985) show the structure of the radial fibres of *Polyorchis penicillatus* (Fig. 9). It is evident from the figure that the radial fibres consist of a bundle of axially oriented, high aspect ratio, parallel microfibrils. The cross section shows that the bundle is densely packed with a volume fraction of microfibrils between 70 and 80%. Reber-Müller et al. (1995) showed the fibres to be rich in fibrillin, and the beaded structure of fibrillin microfibrils (Kielty et al., 2003) is evident in the longitudinal section. It is not clear from Weber and Schmid (1985) whether or not there is a matrix material in the space between the microfibrils.

Material properties

To develop a mechanical model of the composite, we need

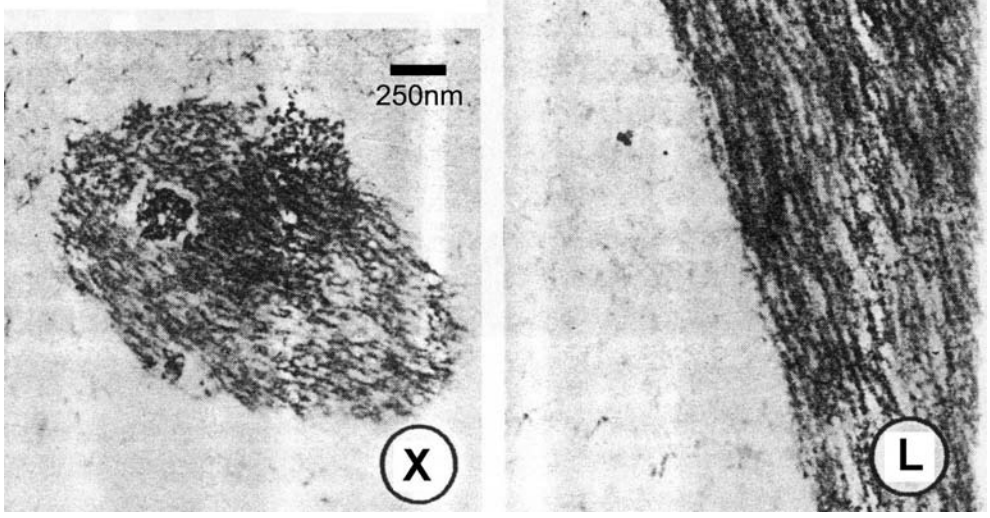

Fig. 9. SEM micrographs from Weber and Schmid (1985) showing longitudinal (L) and cross (X) sections of *Polyorchis* radial fibres. Note the beaded appearance of the fibrillin microfibrils in the longitudinal section. The microfibrils are the high aspect ratio filaments arranged axially with large regions of overlap. The cross section shows the fibre to be a densely packed bundle of microfibrils, with a volume fraction of 70–80%. It is not possible to determine whether individual microfibrils span the entire length of the fibre, but this seems unlikely. No interfibrillar material is obvious in the SEM, but we cannot rule out the possibility that a matrix might exist that did not stain in Weber and Schmid's preparation. We therefore present two possible composite models of the fibre mechanics: a parallel model in which the microfibrils either span the entire length of the fibre, or are cross-linked such that they behave effectively as if they did, and a series model in which the microfibrils transmit axial loads through interfibrillar shear. Reproduced from Weber and Schmid (1985) with permission from Elsevier. Scale bar, 250 nm.

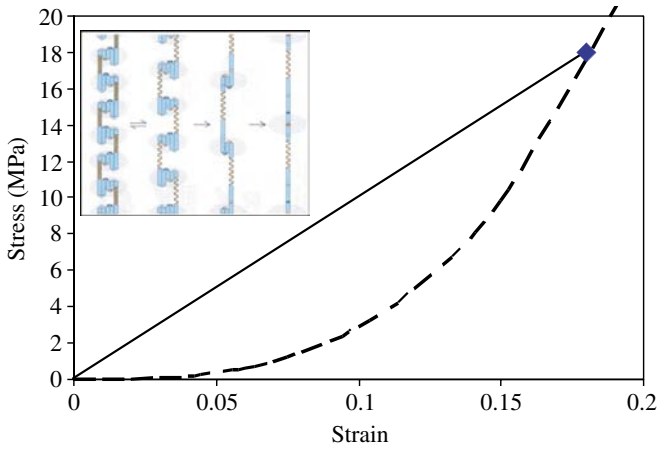

Fig. 10. Stress–strain data for individual fibrillin microfibrils, reproduced from Sherratt et al. (2003). The diamond is their data point, and the solid line their linear interpretation of the mechanical behaviour. The broken curve is another valid interpolation, suggested by the molecular structure of fibrillin (Sherratt et al., 2003), shown in the inset (reproduced with permission from Elsevier). The initial toe region of the J-shaped curve corresponds to molecular unfolding of flexible parts of the fibrillin protein, while the final, much higher stiffness region probably arises from the deformation of rigid, globular domains in the protein.

information on the material properties of the constituent components. Sherratt et al. (2003) used molecular combing experiments to calculate a stiffness approaching 100 MPa for the component microfibrils. They modelled the microfibrils as linear springs, but it is certainly possible, indeed likely, that the mechanical behaviour of fibrillin microfibrils is not linear, but quite non-linear, or J-shaped. Many biological materials exhibit this type of behaviour. At low extensions, there are no tight constraints and the resistance is entropy-based on orientation and conformation, so modulus is low; at high extensions, there is much orientation, and forces pull against the constraining molecular bonds, so modulus is high. To illustrate this, we have drawn a J-shaped curve in Fig. 10. The diamond represents the single stress value (approximately 18 MPa) reported by Sherratt et al. (2003). The 78–96 MPa stiffness reported was based on the assumption that the stress rose linearly from zero. But if our J-curve correctly represents the fibrillin microfibril behaviour, then it actually exhibits stiffnesses both lower and higher than their reported value. Fibrillin is a globular protein (Kielty et al., 2003), so it seems reasonable to think that microfibrils made of fibrillin might behave similarly to actin filaments, which are known to have a tensile stiffness of approximately 2.5 GPa (Gittes et al., 1993; Kojima et al., 1994). This suggests that the stiffness at 18 MPa on the postulated J-shaped stress–strain curve (Fig. 10) might be more than an order of magnitude greater than the secant stiffness calculated by Sherratt et al. (2003). If this is true, then the stiffness at the initial toe region of the J-curve (Fig. 10) would be an order of magnitude or more lower than their estimate, or ~10 MPa or less.

A further reinterpretation of the data presented by Sherratt et al. (2003) comes in their calculation of the strain experienced by the microfibrils during their experiments. They based their calculation of the strain on the displacement of fibrillin beads, as seen with their atomic force microscope, from approximately 59 nm to approximately 70 nm. They calculate the strain in the microfibrils as (70–59)/59=0.186. However, in their X-ray diffraction data (fig. 1 in Sherratt et al., 2003), they show that the zonule fibres must be stretched to a strain of 2 in order for the bead separation to reach 70 nm. Thus, there appears to be an order of magnitude difference between the whole zonule fibre strain and the microfibril inter-bead strain. If this is true, and if we consider fibrillin microfibrils to have a J-shaped curve, then it is possible that the microfibril stiffness could be as low as 1 MPa.

Although we believe each step in our reinterpretation of the data presented by Sherratt et al. (2003) is reasonable, we cannot conclude definitively whether 1 MPa or 100 MPa best represents the stiffness of the microfibrils. Therefore, we must consider both as possible, and assess what we can infer about the fibres' structure and elasticity.

Composite models

Based on the structure shown by Weber and Schmid (1985), we model the elastic fibre as a fibre-reinforced composite. There are three possible arrangements of the microfibrils and matrix in the composite. The first possibility is that the microfibrils are continuous, extending the full length of the fibre, arranged in parallel. This is unlikely, given the 3 mm length of the elastic fibres, but it is not impossible. The second is a variation on the first: the microfibrils are structurally discontinuous but functionally continuous because of direct molecular interaction in the form of crosslinks between the microfibrils. The third is that the microfibrils are discontinuous and do not span the full length of the fibre but instead overlap to a degree, transferring axial load in shear through the matrix.

Since the second possibility is a variation on the first, we will consider them together. Thus, we have two hypotheses to investigate: functionally continuous microfibrils or discontinuous microfibrils in which the load is transferred through a matrix. It is clear that if there is no matrix, a discontinuous model cannot work. Considering the discussion earlier about the modulus of the microfibrils, each of the two hypotheses must be modelled with two values for the microfibril stiffness.

Test hypotheses

Case 1. Functionally continuous and 100 MPa

In this model, we consider the fibres to be a parallel composite with stiff reinforcing fibres. Relabelling terms to represent the components of the radial fibres (matrix and cross-linked microfibril bundles) and rearranging, Eqn 2 becomes:

$$E_m = (E_f - E_{\mu f}V_{\mu f})/(1 - V_{\mu f}) , \quad (5)$$

where E_f is the stiffness of the radial fibres (measured earlier to be approximately 0.9 MPa), $E_{\mu f}$ is the stiffness of the microfibrils [reported by Sherratt et al. (2003) to be

78–96 MPa], and $V_{\mu f}$ is the volume fraction of microfibrils in the radial fibre (70–80%; Fig. 9). If the values for E_f, $E_{\mu f}$ and $V_{\mu f}$ are substituted into Eqn 5, E_m is predicted to be negative, which is impossible. We therefore reject this hypothesis.

Case 2. Functionally continuous and 1 MPa

We use the same mechanical model here as in the first case but come at the problem from a different angle. If our measurement of the fibre stiffness is correct (and its similarity to the stiffness of other fibrillin-rich fibres – Table 4 – suggests that it is), then the requirement in Eqn 5 that $E_m \geqslant 0$ requires that the microfibrils have a maximum modulus of 1.28 MPa ($V_{\mu f}$=70%). Even if the volume fraction is assumed to be as low as 50%, the maximum $E_{\mu f}$ must be less than 1.8 MPa. These values are so close to the reinterpreted value of the microfibril modulus that we cannot reject this hypothesis.

Case 3. Discontinuous and 100 MPa

It is possible that the radial fibres are structured more like a series composite. That is to say, the stress is transferred from one microfibril to the next in shear through a soft matrix. It is obvious that the microfibrils overlap to a great degree, so the strict series (Reuss) model is not likely to be applicable. However, we can use Cox's model of an aligned discontinuous fibre composite (Cox, 1952). Given the data we have about the morphology of the fibre, we choose to formulate Cox's model following Jackson et al. (1988):

$$E_f = V_{\mu f}E_{\mu f}\left[1 - \frac{\tan h(u)}{u}\right] + (1-V_{\mu f})E_m ,$$

$$\text{where} \qquad u = s\sqrt{\frac{G_m V_{\mu f}}{E_{\mu f}(1-V_{\mu f})}} , \qquad (6)$$

where s is the aspect ratio of the microfibrils, G_m is the shear modulus of the matrix, and all other parameters are as defined earlier. We do not have a measurement of the aspect ratio of the jellyfish microfibrils, but Sherratt et al. (2003) reported an aspect ratio of approximately 100 for the microfibrils in the bovine eye, and this does not seem inconsistent with Weber and Schmid's SEM of jellyfish microfibrils (Fig. 9; Weber and Schmid, 1985). The shear modulus is the remaining parameter. If we assume the hypothetical matrix to be mechanically similar to elastin (G ~500 kPa), then with $E_{\mu f}$=100 MPa, the model predicts a fibre stiffness of 70 MPa, nearly two orders of magnitude greater than our measured value. Even if we posit a shear modulus of 0.1 kPa, 5000 times lower than the stiffness of elastin, the model still predicts a fibre stiffness greater than 40 MPa. We therefore reject this hypothesis.

Case 4. Discontinuous and 1 MPa

We use the same mechanical model as in Case 3 but with much more compliant microfibrils. Using our reinterpreted microfibril modulus of approximately 1 MPa, a matrix shear modulus of 1 kPa is required to obtain an overall fibre modulus of 0.9 MPa. This is well within the realms of possibility, so we cannot reject this hypothesis.

Although we cannot reject Case 4, we think it unlikely, as there does not appear to be any matrix material between the fibres (Fig. 9; Weber and Schmid, 1985). It is however possible that there is a matrix material present in the elastic fibres, which did not stain in Weber and Schmid's preparation. Reber-Müller et al. (1995, 1996) suggested this possibility, although Schmid et al. (1999) suggested that the microfibrils alone were responsible for the observed elasticity of the fibres. It seems more likely that the functionally continuous model is correct, particularly given the high volume fraction and high degree of overlap of the microfibrils in the fibre and observations by several authors of irreversible transglutaminase-derived crosslinks between fibrillin-rich microfibrils in several systems (Thurmond and Trotter, 1996; Qian and Granville, 1997; Schittny et al., 1997; Kielty et al., 2002). In either case, however, we conclude that the modulus of the microfibrils must be much less than the 78–96 MPa reported by Sherratt et al. (2003) and that it should be of the order of 1 MPa.

Low modulus behaviour of fibres

Evidence that the jellyfish fibres are showing rubber-like entropic elasticity can be extracted from a comparison of Wright et al. (1999) and Sherratt et al. (2003). The extremely low initial stiffness behaviour for zonule fibres reported by Wright et al. (1999) and the initial part of the zonule strain *vs* bead periodicity data (30–50% zonule strain with no change in bead periodicity) reported by Sherratt et al. (2003) could arise from the microfibrils being slack and wavy and as a consequence of exhibiting conformational entropy on their own. For this to happen, the only requirement is that the persistence length of the microfibrils must be less than the total contour length between junction points. If this is the case, then the microfibrils can act as an entropic chain and give low stiffness elasticity. That this is possible, indeed probable, is documented in the AFM (atomic force microscope) figure presented by Sherratt et al. (2003), which shows the contour of a single microfibril from their combing experiments. The control sample, presumably a microfibril that was just allowed to bind to the mica surface without the flow-induced 'combing', is strongly coiled, indicating that it is very flexible. From this we can only conclude that the persistence length of microfibrils is much less than their contour lengths, and hence that they can act as entropic chains.

At very low extension, then, jellyfish fibres are likely to be extremely compliant. However, when extended further (30% or more), it is likely that the component microfibrils are becoming extended in the direction of the applied strain, and the fibre stiffness rises due to a non-Gaussian stiffening of the coiled microfibrils. As the fibres are stretched further, we suggest that the microfibrils themselves are being stretched. The role of the substantial pre-strain we calculate for fibres *in vivo* would therefore be to straighten the microfibrils and hence increase the stiffness to a level useful for storing energy.

Energetics

Whatever the source of the elasticity, with the measured stiffness of the fibres it is possible to determine whether the fibres alone are sufficient to account for the energy required to refill the bell. Elastic energy (W) is the integral of the elastic restoring force (F) over the distance stretched (x):

$$W = \int F\mathrm{d}x \, . \tag{7}$$

Expressed in terms of stress (σ) and strain (ϵ), this becomes:

$$W = \int \sigma(\epsilon) A l_0 \mathrm{d}\epsilon \, , \tag{8}$$

where A is the area over which the force is applied and l_0 is the resting wall thickness. The area of interest here is the inner surface of the bell, A_u, where:

$$A_\mathrm{u} = 2\pi r_\mathrm{m} h_\mathrm{s} \tag{9}$$

and r_m is the radius of the subumbrellar cavity and h_s is the shoulder height of the jellyfish. For the jellyfish in Fig. 8B (individual 25; bell height = 22.1 mm), the total subumbrellar area is 3.3×10^{-4} m^2. Gladfelter (1972) described three regions in the bell: ad-, per- and inter-radii. Assigning equal areas (A_i) and initial thicknesses ($l_{0,\mathrm{i}}=\tau$) to the three regions, the integral becomes:

$$W = \sum_{regions,i} A_\mathrm{i}\tau \int_0^{\epsilon_\mathrm{i}} \sigma(\epsilon)\mathrm{d}\epsilon \, , \tag{10}$$

where the ϵ_is are the local radial strains in each region. For the animal in Fig. 8B, each subarea (A_i) is 1.1×10^{-4} m^2 and the initial thickness is 2.9×10^{-3} m. The upper limits of integration are obtained from Gladfelter's measurements of the radial strain in the three regions (Gladfelter, 1972). These were: 36%, 34% and 16% in the per-, inter- and ad-radii, respectively. The functional form of $\sigma(\epsilon)$ is given by Eqn 2. Neglecting the contribution of the mesogleal matrix for the moment, substituting into Eqn 9 and simplifying gives:

$$W = \tfrac{1}{3}A_\mathrm{u}\tau E_\mathrm{f} V_\mathrm{f}\left[\int_0^{0.34}\epsilon\mathrm{d}\epsilon + \int_0^{0.36}\epsilon\mathrm{d}\epsilon + \int_0^{0.16}\epsilon\mathrm{d}\epsilon\right] = 35.3\ \mu\mathrm{J} \, . \tag{11}$$

The resilience of the mesogleal bell was calculated by DeMont and Gosline (1988a) to be 0.58, so the total energy that can be released from the fibres is 20 μJ, which is sufficient to meet the 17 μJ of energy estimated by DeMont and Gosline (1988b) to be required to refill the bell of a similarly sized animal (bell height = 2 cm). The model assumes that all of the fibres are aligned perfectly with the local stress axis and that they are all strained maximally. This will, of course, not be the case generally, so the total energy available will be somewhat less. However, the resilience value of 0.58 was probably an underestimate of the true resilience of the intact structure since it was calculated from isolated tissue preparations whose properties will have been affected by water leakage from the sample.

In his analysis of the deformation of the animal, Gladfelter (1972) showed that the presence of the joint mesoglea substantially reduced the radial strain relative to a hypothetical unjointed animal of otherwise identical resting dimensions. He concluded that the joints existed to allow the animal to make a contraction of given magnitude for less input force. DeMont and Gosline (1988a) measured the non-linear stiffness of the intact mesogleal bell. They took Gladfelter's argument further, suggesting that the non-linear elasticity allowed the muscle to power the refilling stage by storing energy at a time in the jet phase when it is not useful for generating thrust (DeMont and Gosline, 1988b). We have shown that the radial fibres are stiff enough on their own to store the energy required to refill the bell. This allows the joint mesoglea to be much more compliant, which reduces the cost of locomotion by reducing the opposition to thrust development.

This work was supported by research grants from the Natural Sciences and Engineering Research Council of Canada, the Zoology Department of the University of British Columbia and the Coastal Ecosystems Research Foundation. The authors would like to thank the staff and divers of the Bamfield Marine Sciences Centre and Westwind Sealab Supplies for collecting specimens. Special thanks are owed to Margo Lillie for assistance with the interpretation of the mechanical testing data and to Tara Law for accommodation during an extended stay in Bamfield. Margo Lillie, Julian Vincent and three anonymous reviewers provided well-appreciated comments on earlier drafts of this manuscript. The authors would also like to acknowledge the assistance of the Statistical Consulting Service of the University of Wollongong with the analysis of the data.

References

Aaron, B. B. and Gosline, J. M. (1981). Elastin as a random-network elastomer: a mechanical and optical analysis of single elastin fibres. *Biopolymers* **20**, 1247-1260.

Alexander, R. McN. (1962). Visco-elastic properties of the body-wall of sea anemones. *J. Exp. Biol.* **39**, 373-386.

Arai, M. and Brinckmann-Voss, A. (1980). The hydromedusae of British Columbia and Puget Sound. *Can. Bull. Fish. Aquat. Sci.* **204**, 1-192.

Baldock, C., Koster, A. J., Ziese, U., Sherrattt, M. J., Kadler, K. E., Shuttleworth, C. A. and Kielty, C. M. (2001). The supramolecular organisation of fibrillin-rich microfibrils. *J. Cell Biol.* **152**, 1045-1056.

Beck, K., McCarthy, R. A., Chiquet, M., Masuda-Nakagawa, L. and Schlage, W. K. (1989). Structure of the basement membrane protein laminin: variations on a theme. In *Cytoskeletal and Extracellular Proteins: Structure, Interactions and Assembly* (ed. U. Aebi and J. Engel), pp. 102-105. New York: Springer Verlag.

Bouillon, J. and Coppois, G. (1977). Étude comparative de la mésoglée des cnidaires. *Cah. Biol. Mar.* **18**, 339-368.

Bouillon, J. and Vandermeerssche, G. (1957). Structure et nature de la mésoglée des hydro- et scyphoméduses. *Ann. Soc. Roy. Zool. Bel.* **87**, 9-25.

Brinckmann-Voss, A. (2000). The hydroid and medusa of *Sarsia bella* sp nov (Hydrozoa, Anthoathecatae, Corynidae), with a correction of the "life cycle" of *Polyorchis penicillatus* (Eschscholtz). *Sci. Mar.* **64**, 189-195.

Chapman, G. (1959). The mesoglea of *Pelagia noctiluca*. *Q. J. Microsc. Sci.* **100**, 599-610.

Chapman, G. (1966). The structure and functions of the mesoglea. *Symp. Zool. Soc. Lond.* **16**, 147-168.

Colin, S. P. and Costello, J. H. (2002). Morphology, swimming performance and propulsive mode of six co-occurring hydromedusae. *J. Exp. Biol.* **205**, 427-437.

Cox, H. L. (1952). The elasticity and strength of paper and other fibrous materials. *Br. J. Appl. Phys.* **3**, 72-79.

Davison, I. G., Wright, G. M. and DeMont, M. E. (1995). The structure and physical properties of invertebrate and primitive vertebrate arteries. *J. Exp. Biol.* **198**, 2185-2196.

DeMont, M. E. (1986). Mechanics of jet propulsion in a hydromedusean jellyfish. Doctoral dissertation, University of British Columbia, Vancouver, Canada.

DeMont, M. E. and Gosline, J. M. (1988a). Mechanics of jet propulsion in the hydromedusan jellyfish, *Polyorchis penicillatus*. I. Mechanical properties of the locomotor structure. *J. Exp. Biol.* **134**, 313-332.

DeMont, M. E. and Gosline, J. M. (1988b). Mechanics of jet propulsion in the hydromedusan jellyfish, *Polyorchis penicillatus*. II. Energetics of the jet cycle. *J. Exp. Biol.* **134**, 333-345.

DeMont, M. E. and Gosline, J. M. (1988c). Mechanics of jet propulsion in the hydromedusan jellyfish, *Polyorchis penicillatus*. III. A natural resonating bell: The presence and importance of a resonant phenomenon in the locomotor structure. *J. Exp. Biol.* **134**, 347-361.

Dixon, W. J. and Massey, F. J. (1983). *Introduction to Statistical Analysis*. London: McGraw-Hill.

Eriksen, T. A., Wright, D. M., Purslow, P. P. and Duance, V. C. (2001). Role of Ca^{2+} for the mechanical properties of fibrillin. *Proteins* **45**, 90-95.

Faury, G. (2001). Function-structure relationship of elastic arteries in evolution: from microfibrils to elastin and elastic fibres. *Pathol. Biol. (Paris)* **49**, 310-325.

Gittes, F., Mickey, B., Nettleton, J. and Howard, J. (1993). Flexural rigidity of microtubules and actin filaments measured from thermal fluctuations in shape. *J. Cell Biol.* **120**, 923-934.

Gladfelter, W. B. (1972). Structure and function of the locomotory system of *Polyorchis montereyensis* (Cnidaria, Hydrozoa). *Helgoland. Wiss. Meer.* **23**, 38-79.

Gladfelter, W. B. (1973). A comparative analysis of the locomotory systems of medusoid Cnidaria. *Helgoland. Wiss. Meer.* **25**, 228-272.

Gosline, J. M. and DeMont, M. E. (1985). Jet-propelled swimming in squids. *Sci. Am.* **252**, 96-103.

Jackson, A. P., Vincent, J. F. V. and Turner, R. M. (1988). The mechanical design of nacre. *Proc. R. Soc. Lond. B Biol. Sci.* **234**, 415-440.

Keene, D. R., Maddox, B. K., Kuo, H. J., Sakai, L. Y. and Glanville, R. W. (1991). Extraction of extendable beaded structures and their identification as fibrillin-containing extracellular matrix microfibrils. *J. Histochem. Cytochem.* **38**, 441-449.

Kielty, C. M., Sherrattt, M. J. and Shuttleworth, C. A. (2002). Elastic fibres. *J. Cell Sci.* **115**, 2817-2828.

Kielty, C. M., Baldock, C., Sherrattt, M. J., Rock, M. J., Lee, D. and Shuttleworth, C. A. (2003). Fibrillin: from microfibril assembly to mechanical function. In *Elastomeric Proteins: Structures, Biomechanical Properties and Biological Roles* (ed. P. R. Shewry, A. S. Tatham and A. J. Bailey), pp. 94-114. Cambridge: Cambridge University Press.

Kojima, H., Ishijima, A. and Yanagida, T. (1993). Direct measurement of stiffness of single actin filaments with and without tropomyosin by *in vitro* manipulation. *Proc. Natl. Acad. Sci. USA* **91**, 12962-12966.

Lillie, M. A., Chalmers, G. W. and Gosline, J. M. (1994). The effects of heating on the mechanical properties of arterial elastin. *Connect. Tissue Res.* **31**, 23-35.

Lillie, M. A., David, G. J. and Gosline, J. M. (1998). Mechanical role of elastin-associated microfibrils in pig aortic elastic tissue. *Connect. Tissue Res.* **37**, 121-141.

Lin, Y.-C. J. and Spencer, A. N. (2001). Localisation of intracellular calcium stores in the striated muscles of the jellyfish *Polyorchis penicillatus*: Possible involvement in excitation-contraction coupling. *J. Exp. Biol.* **204**, 3727-3736.

Malak, T. M. and Bell, S. C. (1994). Distribution of fibrillin-containing microfibrils and elastin in human fetal membranes: a novel molecular basis for membrane elasticity. *Am. J. Obstet. Gynecol.* **171**, 195-205.

McConnell, C. J., Wright, G. M. and DeMont, M. E. (1996). The modulus of elasticity of lobster aorta microfibrils. *Experientia* **52**, 918-921.

McConnell, C. J., DeMont, M. E. and Wright, G. M. (1997). Microfibrils provide non-linear elastic behaviour in the abdominal artery of the lobster, *Homarus americanus*. *J. Physiol.* **499**, 513-526.

Megill, W. M. (2002). *The Biomechanics of Jellyfish Swimming*. PhD dissertation, University of British Columbia, British Columbia, Canada.

Milewicz, D. M., Urban, Z. and Boyd, C. (2000). Genetic disorders of the elastic fiber system. *Matrix Biol.* **19**, 471-480.

Qian, R.-Q. and Glanville, R. W. (1997). Alignment of fibrillin molecules in elastic microfibrils is defined by transglutaminase-derived cross-links. *Biochemistry* **36**, 15841-15847.

Reber-Müller, S., Spissinger, T., Schuchert, P., Spring, J. and Schmid, V. (1995). An extracellular matrix protein of jellyfish homologous to mammalian fibrillins forms different fibrils depending on the life stage of the animal. *Dev. Biol.* **168**, 662-672.

Reber-Müller, S., Ono, S., Schuchert, P., Spring, J. and Schmid, V. (1996). Fibrillin in the extracellular matrix of cnidarians: an immunohistochemical approach. *Sci. Mar.* **60**, 55-68.

Rees, J. T. and Larson, R. J. (1980). Morphological variation in the hydromedusa genus *Polyorchis* on the west coast of North America. *Can. J. Zool.* **58**, 2089-2095.

Robinson, P. N. and Godfrey, M. (2000). The molecular genetics of Marfan syndrome and related microfibrillopathies. *J. Med. Genet.* **37**, 9-25.

Sarras, M. P., Madden, M. E., Zhang, X., Gunwar, S., Huff, J. K. and Hudson, B. G. (1991). Extracellular matrix (mesoglea) of *Hydra vulgaris*. I. Isolation and characterization. *Dev. Biol.* **148**, 495-500.

Sarras, M. P., Yan, L., Grens, A., Zhang, X., Agbas, A., Huff, J. K., St John, P. L. and Abrahamson, D. R. (1994). Cloning and biological function of laminin in *Hydra vulgaris*. *Dev. Biol.* **164**, 312-324.

Satterlie, R. A. and Spencer, A. N. (1983). Neuronal control of locomotion in hydrozoan medusae. *J. Comp. Physiol. A* **150**, 195-206.

Schittny, J. C., Paulsson, M., Vallan, C., Burri, P. H., Kedei, N. and Aeschlimann, D. (1997). Protein crosslinking mediated by tissue transglutaminase correlates with the maturation of extracellular matrices during lung development. *Am. J. Respir. Cell Mol. Biol.* **17**, 334-343.

Schmid, V., Ono, S.-I. and Reber-Müller, S. (1999). Cell-substrate interactions in Cnidaria. *Microsc. Res. Tech.* **44**, 254-268.

Shadwick, R. E. and Gosline, J. M. (1981). Elastic arteries in invertebrates: mechanics of the octopus aorta. *Science* **213**, 759-761.

Shadwick, R. E. and Gosline, J. M. (1985). Mechanical properties of the octopus aorta. *J. Exp. Biol.* **114**, 259-284.

Sherrattt, M. J., Baldock, C., Haston, J. L., Holmes, D. F., Jones, C. J. P., Shuttleworth, C. A., Wess, T. J. and Kielty, C. M. (2003). Fibrillin microfibrils are stiff reinforcing fibres in compliant tissues. *J. Mol. Biol.* **332**, 183-193.

Singla, C. L. (1978). Fine structure of the neuromuscular system of *Polyorchis penicillatus* (Hydromedusae, Cnidaria). *Cell Tissue Res.* **193**, 163-174.

Skogsberg, T. (1948). A systematic study of the family Polyorchidae. *Proc. Calif. Acad. Sci.* **26**, 101-124.

Spencer, A. N. (1979). Neurobiology of *Polyorchis*. II. Structure of effector systems. *J. Neurobiol.* **10**, 95-117.

Spencer, A. N. (1995). Modulatory mechanisms at a primitive neuromuscular synapse: Membrane currents, transmitter release and modulation by transmitters in a cnidarian motor neuron. *Am. Zool.* **35**, 520-528.

Thurmond, F. A. and Trotter, J. A. (1996). Morphology and biomechanics of the microfibrillar network of sea cucumber dermis. *J. Exp. Biol.* **199**, 1817-1828.

Weber, C. and Schmid, V. (1985). The fibrous system in the extracellular matrix of hydromedusae. *Tissue Cell* **17**, 811-822.

Wess, T. J., Purslow, P. P., Sherrattt, M. J., Ashworth, J., Shuttleworth, C. A. and Kielty, C. M. (1998). Calcium determines the supramolecular organization of fibrillin-rich microfibrils. *J. Cell Biol.* **141**, 829-837.

Wright, D. M., Duance, V. C., Wess, T. J., Kielty, C. M. and Purslow, P. P. (1999). The supramolecular organisation of fibrillin-rich microfibrils determines the mechanical properties of bovine zonular filaments. *J. Exp. Biol.* **202**, 3011-3020.

Zar, J. H. (1984). *Biostatistical Analysis*, 2nd edition. Englewood Cliffs, NJ: Prentice Hall.